computation

MDPI

Supplementary Materials

In Silico Analysis of Peptide-Based Derivatives Containing Bi-functional Warheads Engaging Prime and Non-Prime Subsites to Covalent Binding SARS-CoV-2 Main Protease (M^{pro})

Simone Brogi [1,*], Sara Rossi [2], Roberta Ibba [2], Stefania Butini [2], Vincenzo Calderone [1], Giuseppe Campiani [2] and Sandra Gemma [2,*]

[1] Department of Pharmacy, University of Pisa, Via Bonanno 6, 56126 Pisa, Italy; simone.brogi@unipi.it; vincenzo.calderone@unipi.it

[2] Department of Biotechnology, Chemistry and Pharmacy, DoE Department of Excellence 2018-2022, University of Siena, via Aldo Moro 2, 53100 Siena, Italy; rossi115@student.unisi.it ; roberta.ibba@unisi.it ; butini3@unisi.it; campiani@unisi.it; gemma@unisi.it

* Correspondence: simone.brogi@unipi.it (Si.B.); gemma@unisi.it (S.G.)

Table of Contents

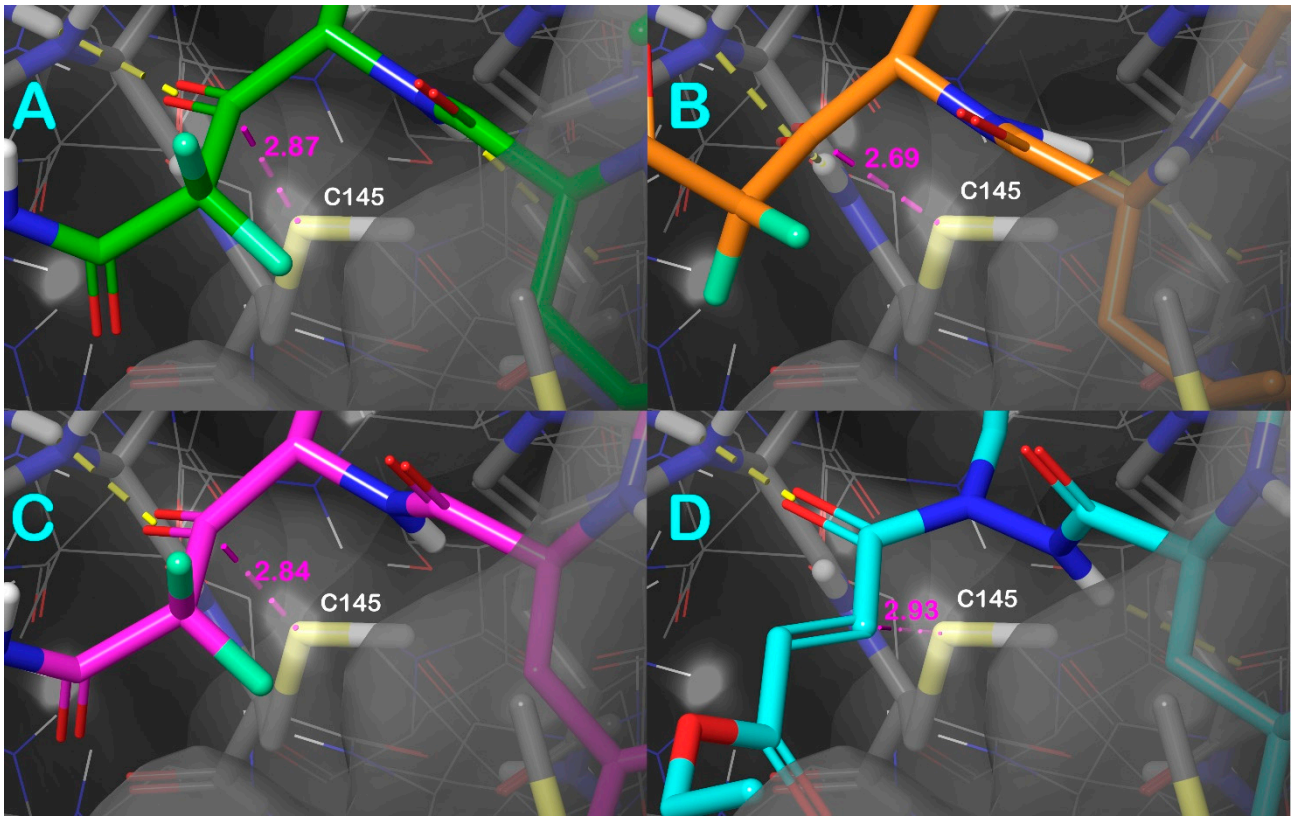

Figure S1. Measured distances between the sulfur of the catalytic residue C145 and the electrophilic carbon of compounds **4** (panel A), **5** (panel B), **6** (panel C), **7** (panel D) that can be susceptible of nucleophilic attack. The measures, visible in magenta, were obtained using the measurement tool available in Maestro. Pictures were generated by Maestro (Maestro, Schrödinger LLC, release 2020-3).

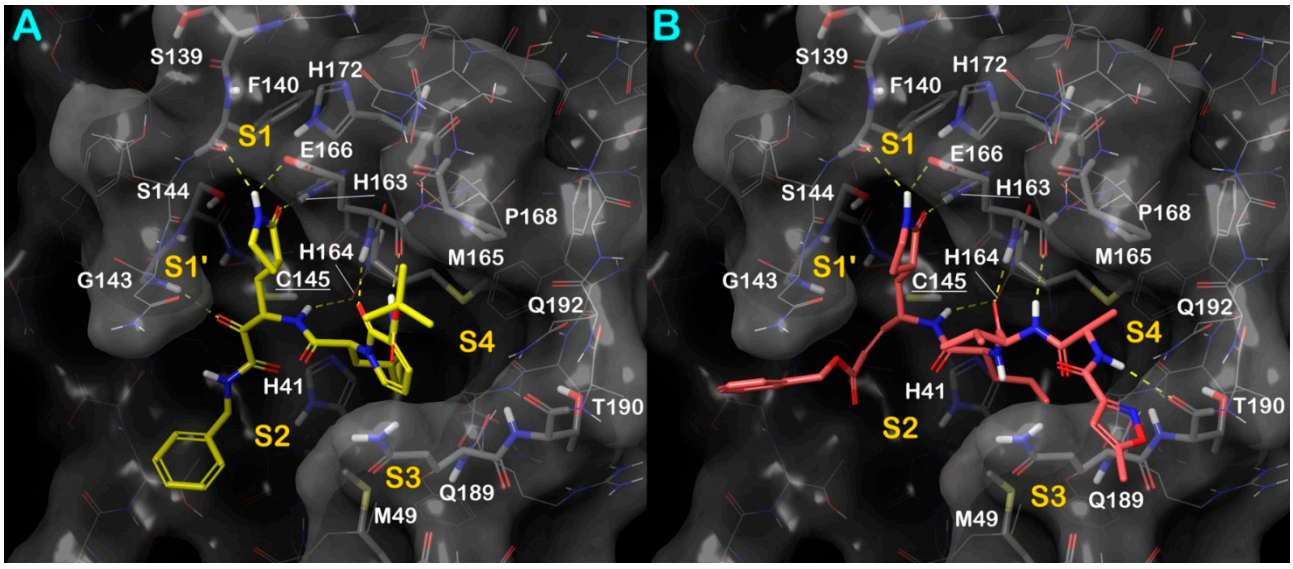

Figure S2. Docked pose of compound **2** and compound **3** (N3) (panel A-B, respectively) into M^{pro}-SARS-CoV-2 (PDB ID 6Y2G). Key interacting residues from different regions are represented by sticks and labelled. H-bonds were represented as yellow dotted lines. Pictures were generated by Maestro (Maestro, Schrödinger LLC, release 2020-3).

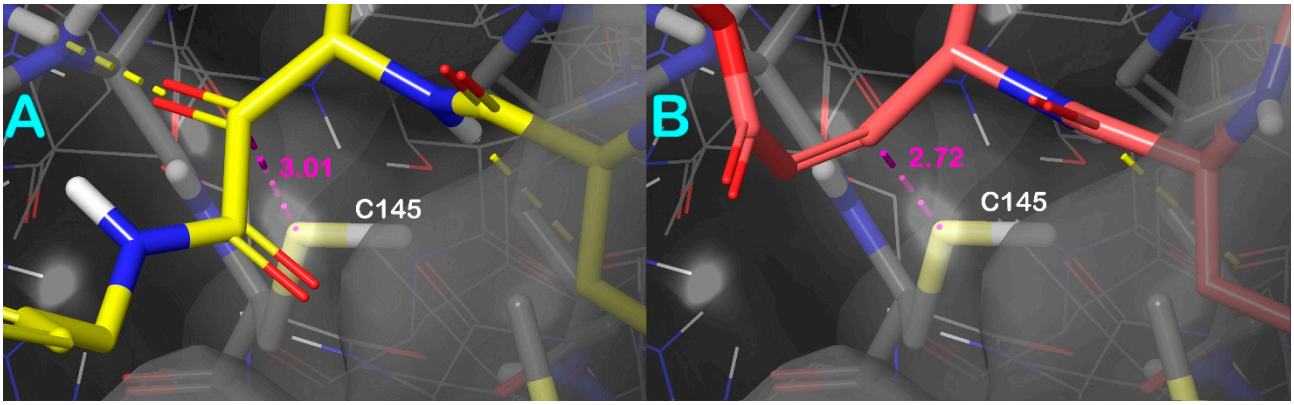

Figure S3. Measured distances between the sulfur of the catalytic residue C145 and the electrophilic carbon of the compound **2** (panel A), and compound **3** (N3) (panel B) that can be susceptible of nucleophilic attack. The measures, visible in magenta, were obtained using the measurement tool available in Maestro. Pictures were generated by Maestro (Maestro, Schrödinger LLC, release 2020-3).

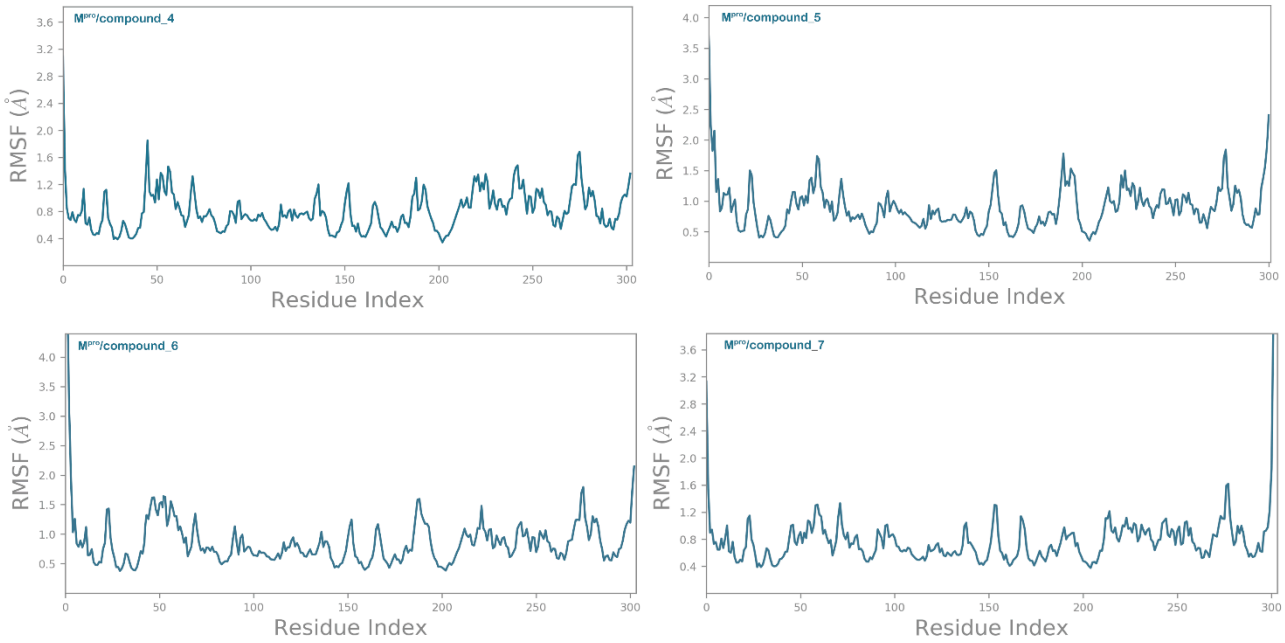

Figure S4. RMSF calculation for each complex, selected by docking studies, after 100 ns of MD simulation. Pictures were generated by Maestro (Maestro, Schrödinger LLC, release 2020-3).

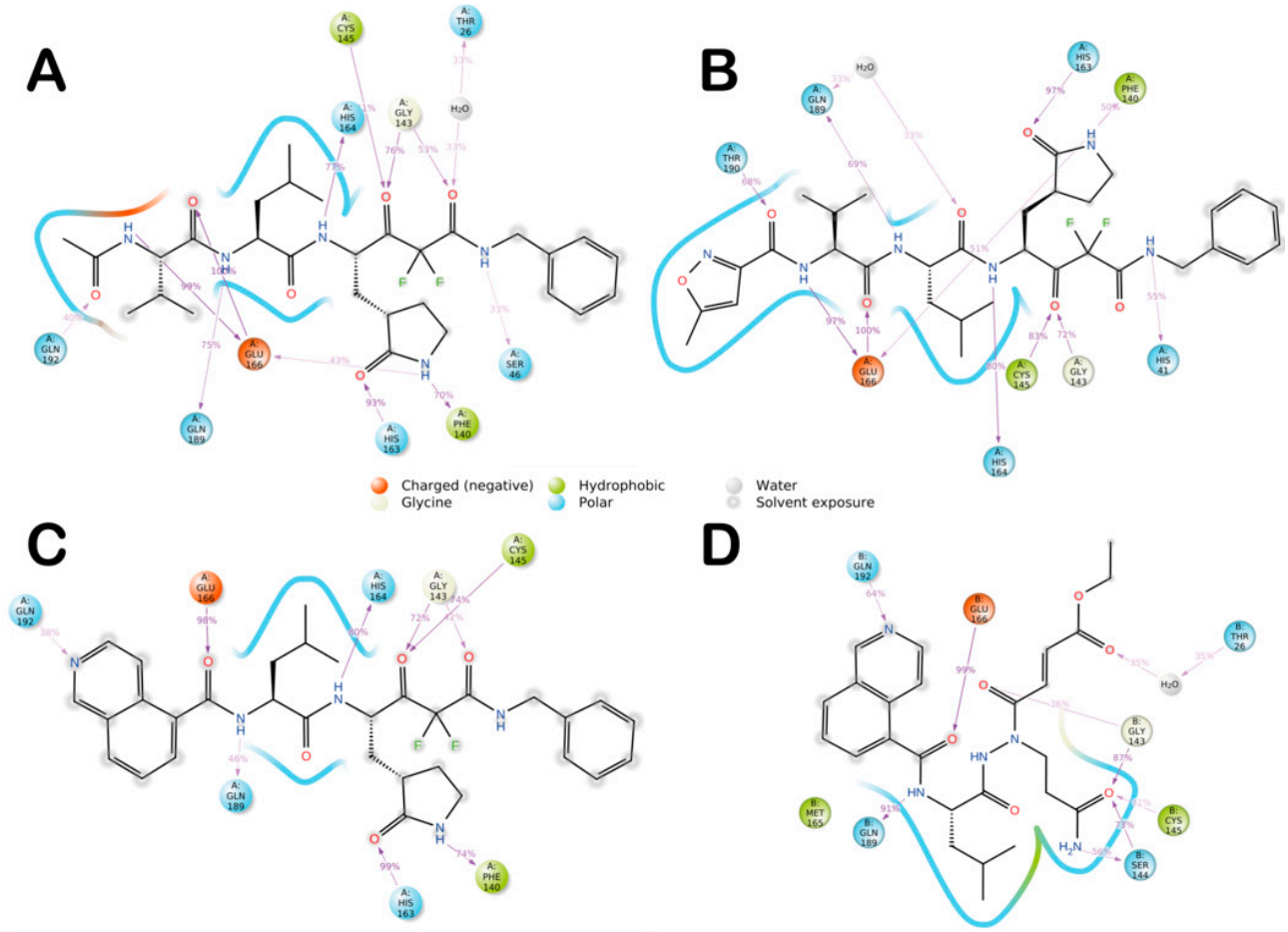

Figure S5. Dynamic ligand-interaction diagram regarding compounds **4** (panel A), **5** (panel B), **6** (panel C), and **7** (panel D) calculated through 100 ns of MD simulation. Dynamic ligand-interaction diagrams were obtained from Maestro. Pictures were generated by simulation interaction diagram available in Desmond via Maestro (Maestro, Schrödinger LLC, release 2020-3).

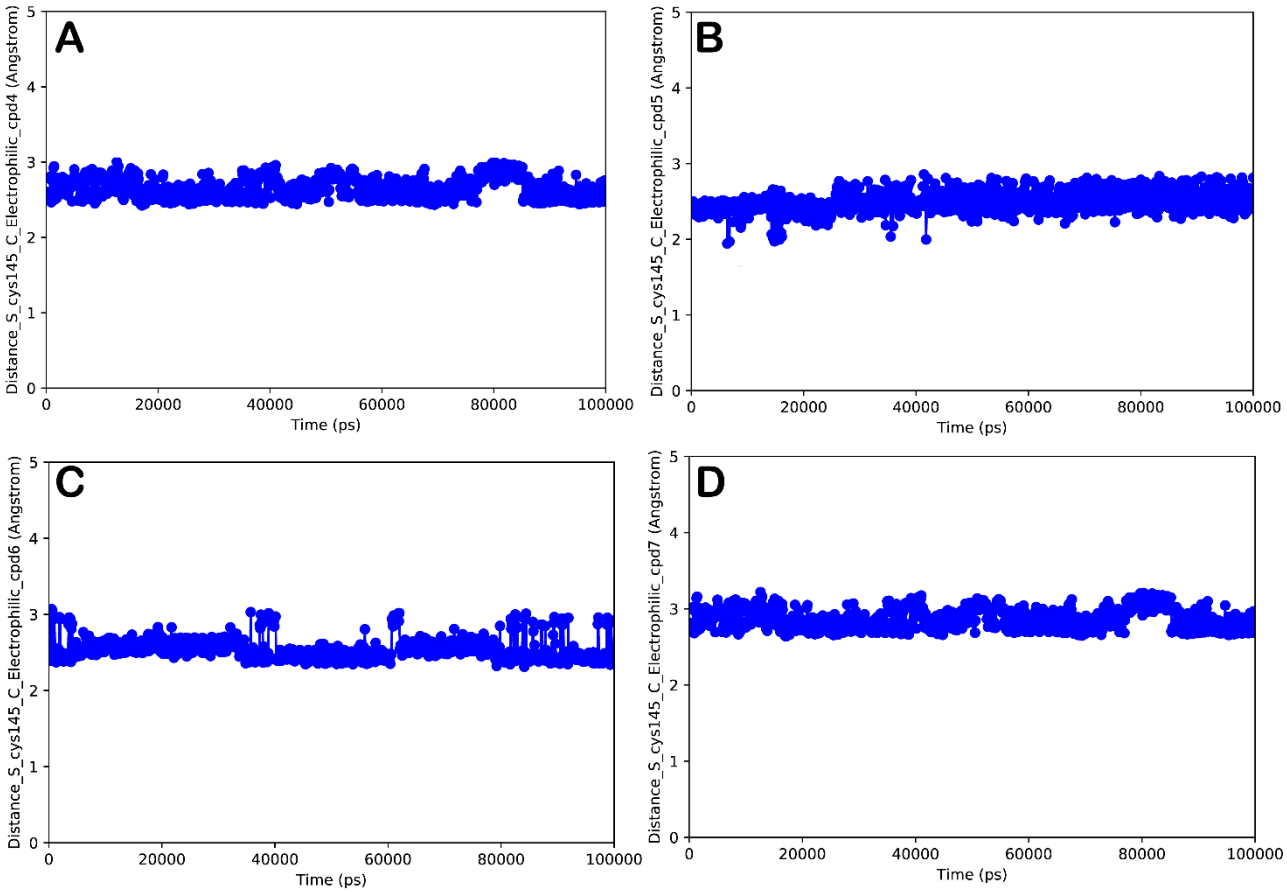

Figure S6. Monitored distances between the sulfur of the catalytic residue C145 and the electrophilic carbon of compounds **4** (panel A), **5** (panel B), **6** (panel C), **7** (panel D) that can be susceptible of nucleophilic attack. The measures were obtained using the measurement tool available in simulation event analysis, which was employed for analyzing MD trajectories. Pictures were generated by Maestro (Maestro, Schrödinger LLC, release 2020-3).

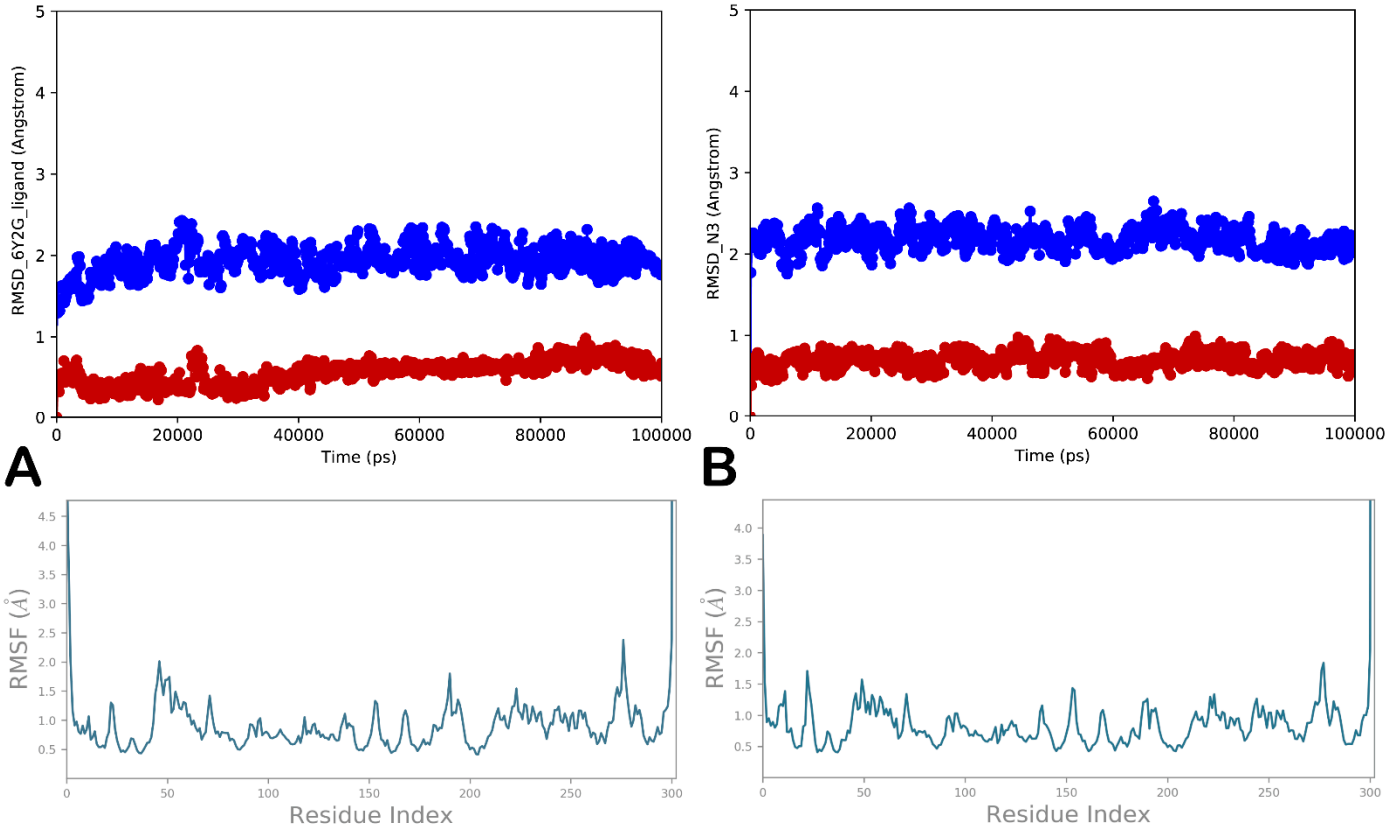

Figure S7. RMSD calculation for each complex investigated in this study: protein (blue line) and ligand (red line); RMSF calculation for each complex, selected by docking studies, after 100 ns of MD simulation (panel A, compound **2**; panel B, compound **3** (N3)). Pictures were generated by Maestro (Maestro, Schrödinger LLC, release 2020-3).

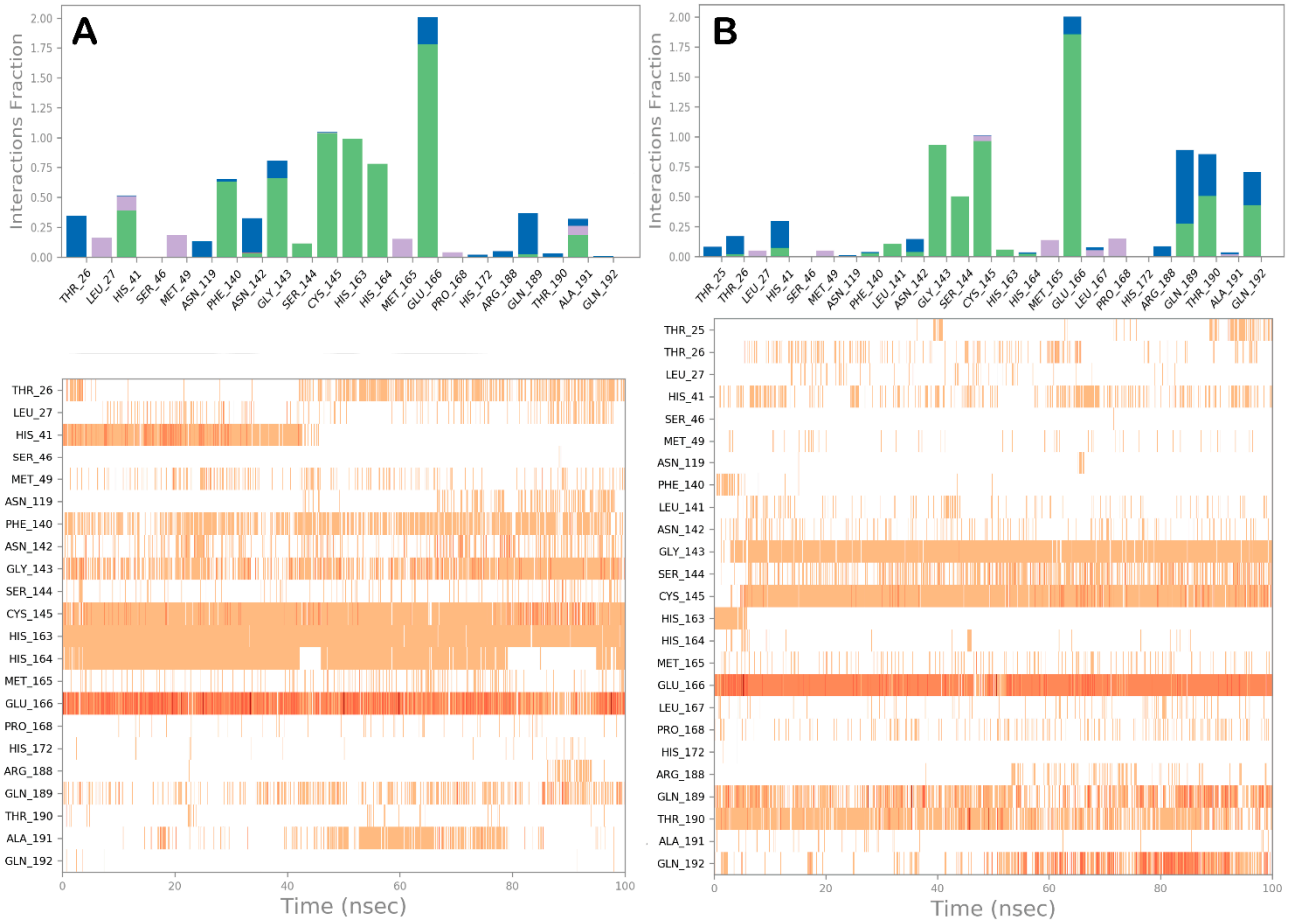

Figure S8. Compound **2** (panel A) and compound **3** (N3) (panel B) monitored during the simulation. The contacts can be grouped by type and summarized, as shown in the plots. Grouping protein-ligand interactions into four types: H-bonds (green), hydrophobic (grey), ionic (magenta), and water bridges (blue). In the second graph of the picture is reported a timeline representation of the contacts. Some residues make more than one specific contact with the ligand, which is represented by a darker shade of orange. Pictures were generated by the simulation interaction diagram available in Desmond via Maestro (Maestro, Schrödinger LLC, release 2020-3).

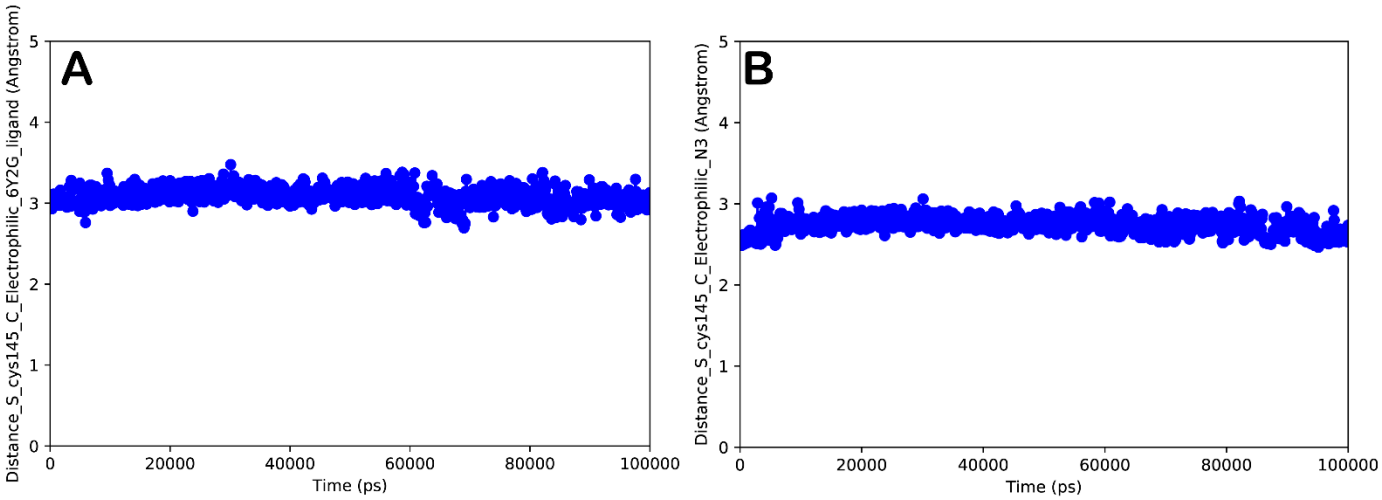

Figure S9. Monitored distances between the sulfur of the catalytic residue C145 and the electrophilic carbon of the compound **2** (panel A) and compound **3** (N3) (panel B), that can be susceptible of nucleophilic attack. The measures were obtained using the measurement tool available in simulation event analysis, which was employed for analyzing MD trajectories. Pictures were generated by Maestro (Maestro, Schrödinger LLC, release 2020-3).

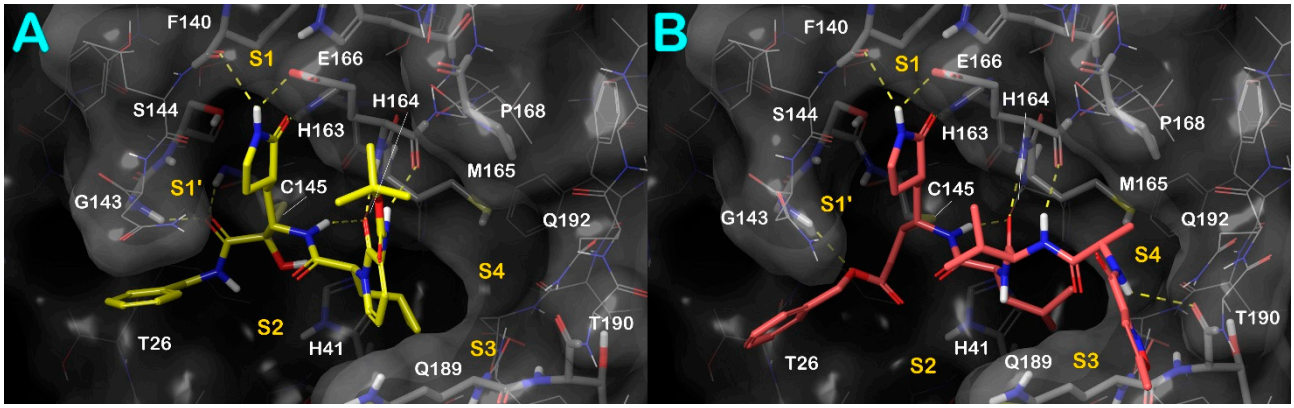

Figure S10. Output regarding the covalent docking investigation considering compound **2** (panel A) and compound **3** (N3) (panel B). Key interacting residues from different regions are represented by sticks and labelled. H-bonds were represented as yellow dotted lines. Pictures were generated by Maestro (Maestro, Schrödinger LLC, release 2020-3).